P10.4 Kelvin-Helmholtz Waves Observed by a Polarimetric Prototype of the WSR-88D Radar

Pengfei Zhang, Alexander Ryzhkov, Dusan Zrnic*

CIMMS, University of Oklahoma, Norman, Oklahoma
*NOAA/National Severe Storms Laboratory, Norman, Oklahoma

1. Introduction

Kelvin-Helmholtz (KH) waves have been observed by human eyes in laboratory and sky, and by weather radar, satellite, profilers, and other meteorological observation instruments in the atmosphere for many years. An observation of Kelvin-Helmholtz (KH) waves made by the dual-polarization KOUN radar and the operational KTLX radar in Oklahoma is studied and presented in this paper. The observed event occurred in stratiform precipitation environment and the radar bright band was embedded within the wind shear layer. The wavelengths and amplitudes of these KH waves are estimated. Wave breaking is also clearly observed. The shear instability is estimated and discussed. Both of dynamical and microphysical features of the KH waves and their environment are examined.

2. Radar observations and analysis

On May 2, 2005, at 08:00 UTC, a large area of stratiform precipitation moved from the west over KTLX and exhibits wave-like features in the reflectivity field. The waves were generated continuously at the west side of KTLX radar. They grew and propagated to the east where they broke. The phenomenon had been observed persistently over 12 hours until the storms moved out of KTLX radar scope and decayed. A vertical cross-section at 16:38 UTC clearly illustrates the wave-like structures (see Fig.1). Starting from 16 UTC to 17 UTC, KOUN radar collected data in full volume scan pattern. Thus, the analysis of three-dimensional polarimetric properties is mainly based on these one hour observations. Potential temperature, wind speed and direction observations of rawinsonde at Norman (OUN) at 12 UTC and NOAA profiler at Purcell (PRC) at 12 UTC and 16 UTC are used as well. The locations of KOUN radar, KTLX radar, OUN sounding station and PRC profiler are also shown in Fig.1.

2.1 Dynamic analysis

The Richardson number

$$Ri = \frac{g}{\theta}\frac{\Lambda\theta}{\Delta Z}\Bigg/\left(\frac{\Delta V}{\Delta Z}\right)^2 \qquad (1)$$

is widely used to estimate stability of a stratified shear flow. Here θ is mean potential temperature, V is mean horizontal velocity, and ΔZ is the depth of shear layer. Theoretical studies show that Ri $\leq$ 0.25 is a necessary condition for shear instability.

For this case, rawinsonde measurements at 12:00UTC and Purcell wind profiler (PRC) observations at 12:00 UTC and 16:00 UTC are used to estimate Ri. The vertical profiles of wind speed, direction, and potential temperature θ. derived from OUN rawinsonde measurements observation (http://weather.uwyo.edu/upperair/sounding.html) at 12 UTC are plotted in Fig.2. It can be seen that the mean wind direction abruptly shifts from 50^{o} below 1.54 km to the opposite direction of 228^{o} above 2.12 km, and is almost unchanged up to 10 km. Potential temperature θ increases almost linearly from 1 km to 10 km. The vertical profiles of wind speed and direction observed by PRC profiler at 12 UTC and 16 UTC show the similar pattern (not shown).

**Corresponding author address*: Pengfei Zhang, CIMMS, University of Oklahoma, Norman, OK 73072; e-mail: pzhang@ou.edu

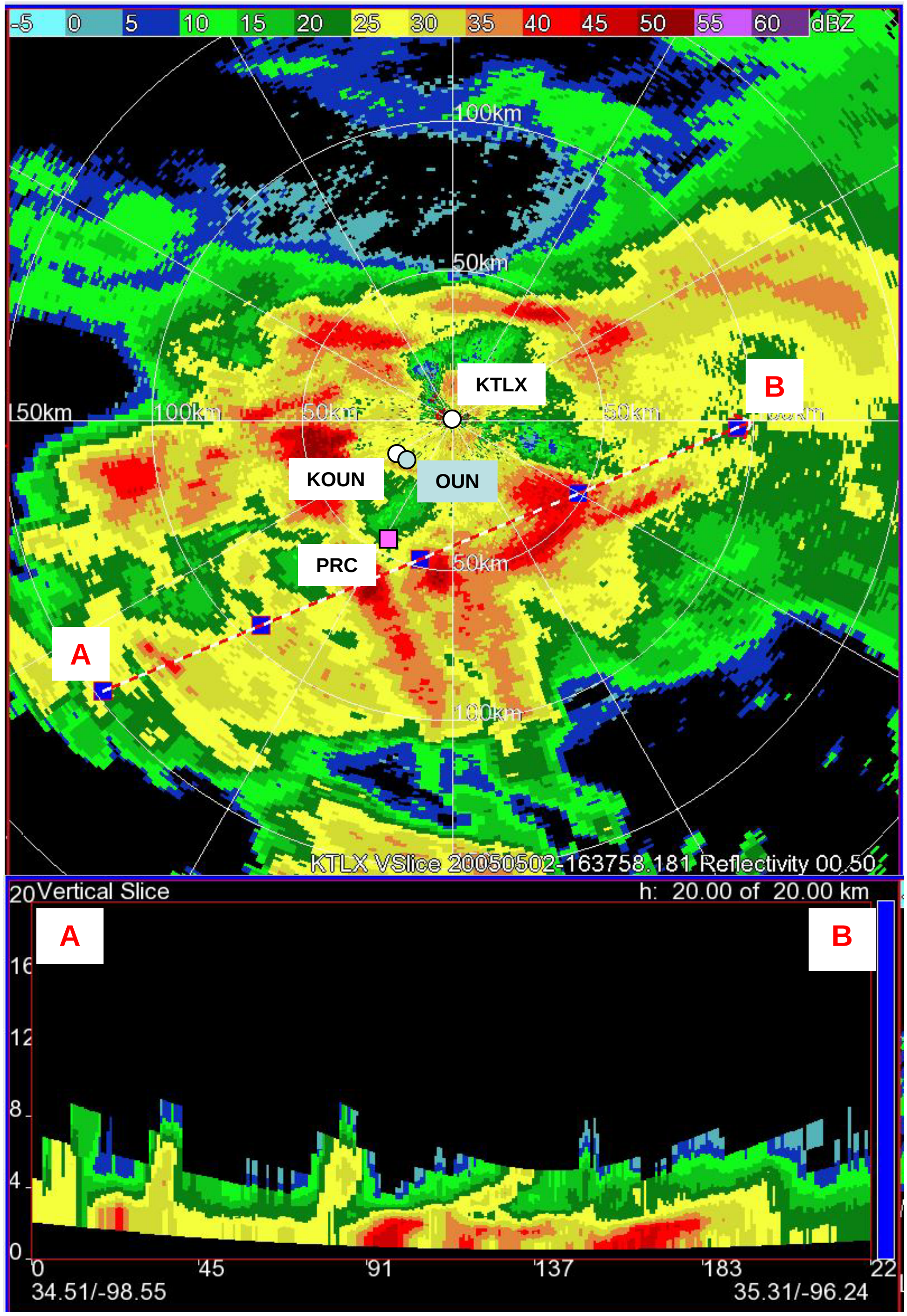

Fig.1 Reflectivity field (upper panel) and correspond vertical cross-section (lower panel) of KTLX radar at 16:37 UTC, 2 May 2005. Range rings are every 50 km and azimuths every 30^{o}. The locations of KTLX radar, KOUN radar, OUN rawinsonde and PRC profiler are marked and labled. The red-white dash line indicates the position of vertical crossection. Two ends of the cross-section is labeled with letter “A” and “B”.

Brown (1980) had discussed the direction and orientation of phase lines of waves with respect to the type of vertical wind shear. In our case, the direction of upper level wind is almost opposite to the one of lower

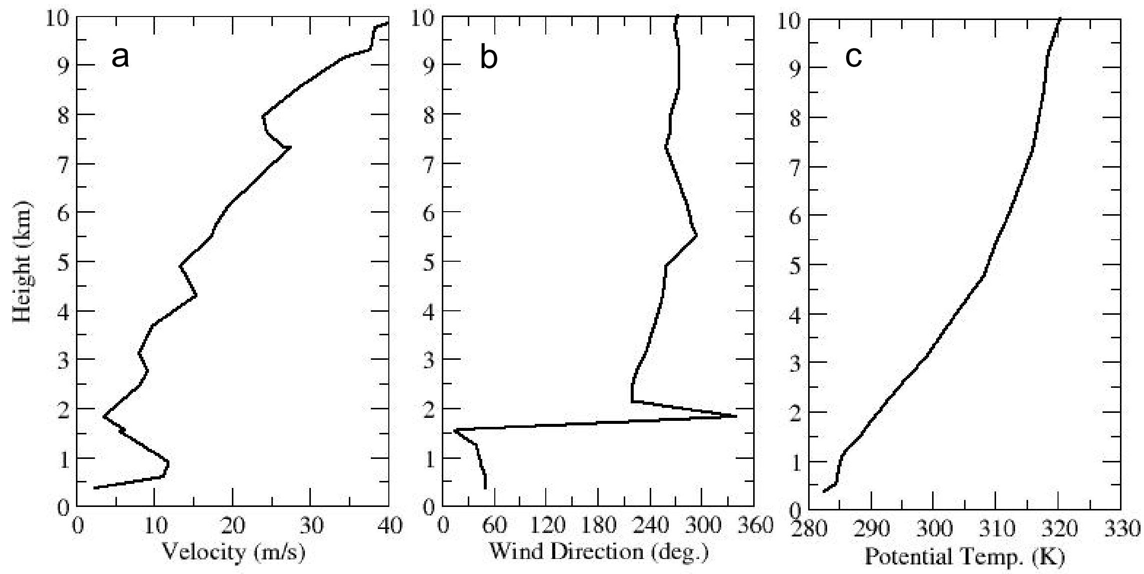

Fig.2 Vertical profiles of (a) wind speed, (b) wind direction, and (c) potential temperature observed at OUN at 12 UTC of 2 May 2005.

level wind. It fits the pure speed shear wind profile described in Brown's review. The observed KH wave rolls are perpendicular to the flow as expected (see Fig.1).

In order to analyze the dynamic and microphysical characteristic of the waves, a vertical cross-section is selected at azimuth 232 ^{o} relative to KOUN radar. It is perpendicular to the phase line of the waves. Then the wind is projected to this cross-section. The vertical profiles of projected wind of rawinsonde and PRC profiler at 12 and 16 UTC are plotted in Fig.3. The PRC profiler observation at 12 UTC shows stronger wind at 3.5 km level than rawinsonde. The projected wind speed reaches 25.4 m/s at 16 UTC that is about 10 m/s higher than the speed at 12 UTC at 4.6 km.

Based on these three wind profiles, the shear layer can be identified between 1 km and 4 km height. Assuming that the potential temperature does not change from 12 UTC to 16 UTC, the three Richardson numbers estimated for this layer are obtained and they are 3.65 (based on rawinsonde at 12 UTC), 2.63 (based on PRC at 12 UTC), and 1.91 (based on PRC at 16 UTC). They are much higher than critical Richardson value of 0.25 for shear instability.

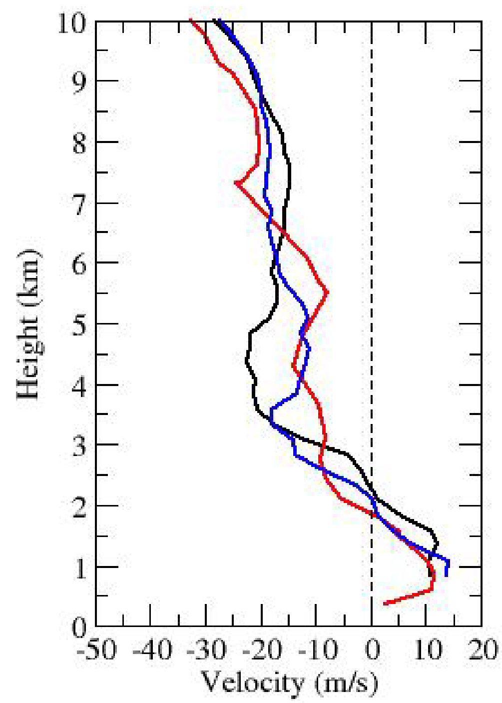

Fig.3 Vertical profiles of the projected wind speed of OUN sounding at 12 UTC (red), PRC at 12 UTC (blue) and PRC at 16 UTC (black).

We have also estimated the local Ri based on observations at adjacent layers. The estimated local maximal wind shear $|\frac{\Delta V}{\Delta Z}|$ is 0.02 s^{-1} at the height of 1.6 km for PRC observation at 16

UTC. The local static stability $\frac{g}{\theta}\frac{\Delta\theta}{\Delta Z}$ at this height is 2.1X10^{-4} s^{-2} estimated from 12 UTC OUN sounding. Thus, Ri is equal to 0.525 which is still higher than 0.25. Browning (1971) had pointed out that there is no evidence to confirm this critical value in the real atmosphere. He has listed the difficulties to accurately estimate Ri in the atmosphere.

Based on numerical calculations, Miles and Howard (1964) found that the relationship between fastest growing wavelength λ of KH wave and sheared layer depth ΔZ is

$$\lambda = 7.5\Delta Z \quad . \qquad (2)$$

The average wavelength estimated from a series of KOUN radar observations at the elevation angle of 1.4^o is about 25 km. The sheared layer depth for this case is 3 km, so the λ/ΔZ is obtained as 8.3. It is close to the Miles and Howard value of 7.5.

Here it is worth mentioning that shallow embedded convection above the freezing level can not occurs because the atmosphere is stable there (see Fig.2). Thus, the observed wave pattern is likely associated with KH waves caused by vertical wind shear rather than convective cells generated by embedded convection aloft (Houze, 1993).

2.2 Stratiform precipitation structure

Houze (1981, 1993) described the basic characteristics of stratiform precipitation in a diagram illustrated in Fig.4. Ice crystals are formed or introduced from outside at the top layer of stratiform cloud. As the ice crystals grow by deposition and fall above the 0^{o}C level, they begin to aggregate and rim to become larger snowflakes with irregular shape. As the aggregated snowflakes fall below 0^{o}C level, they begin to melt and form a melting layer. The mixed-phase hydrometeors in this layer produce a bright band (high reflectivity) in radar reflectivity field. When these hydrometeors fully melted, they become raindrops and fall down to the ground.

In order to analyze the microphysical structure of storm and compare it with the conceptual model, a vertical cross-section is examined in the precipitation region with the horizontal length of 53 km (Fig. 5). This cross-section is in the region where ambient vertical wind shear is weak and KH waves are not pronounced.

Ryzhkov and Zrnic (2003) found that ice crystals are characterized by low reflectivity, high ρ_{hv} and high Z_{dr}. Dry aggregated snow usually produces higher reflectivity, and lower Z_{dr}. Thus, ice crystals and snow can be discriminated by their polarimetric properties. Weak reflectivity, low ρ_{hv}, and high Z_{dr} at top of the cloud in Fig.5 indicate that hydrometeors are predominately ice crystals there. At lower level, Z_{dr} decreases to about 0.8 dB, and reflectivity increases to about 35 dBZ which indicate the transition to aggregated snow. At the very bottom of the cross-section, a layer with high Z_{dr} (~2.5 dB), low ρ_{hv} (~0.90), and high reflectivity (~ 40 dBZ) is clearly observed. This is typical signature of the melting layer. The melting layer in this area of radar echo stretches almost to the ground, hence no clear transition from melting snowflakes to raindrops

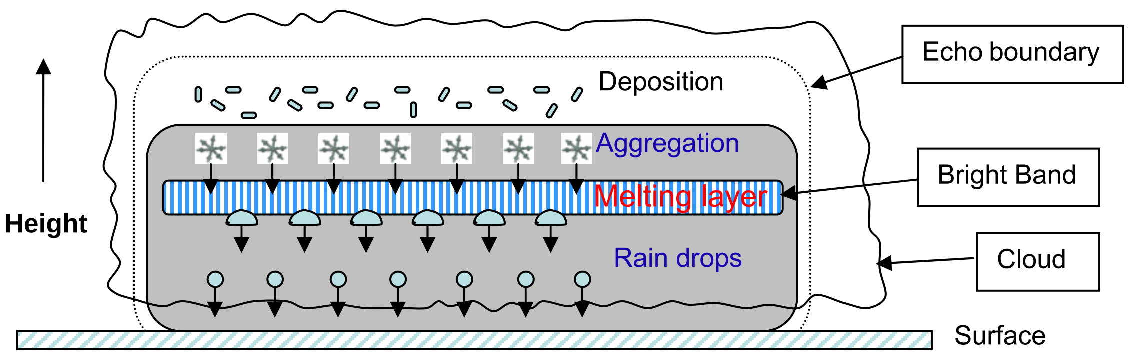

Fig.4 Microphysical structure of stratiform precipitation. Shaded area shows higher reflectivity. Hatched area (blue) indicates melting layer with strongest reflectivity. (Adapted from Houze, 1981)

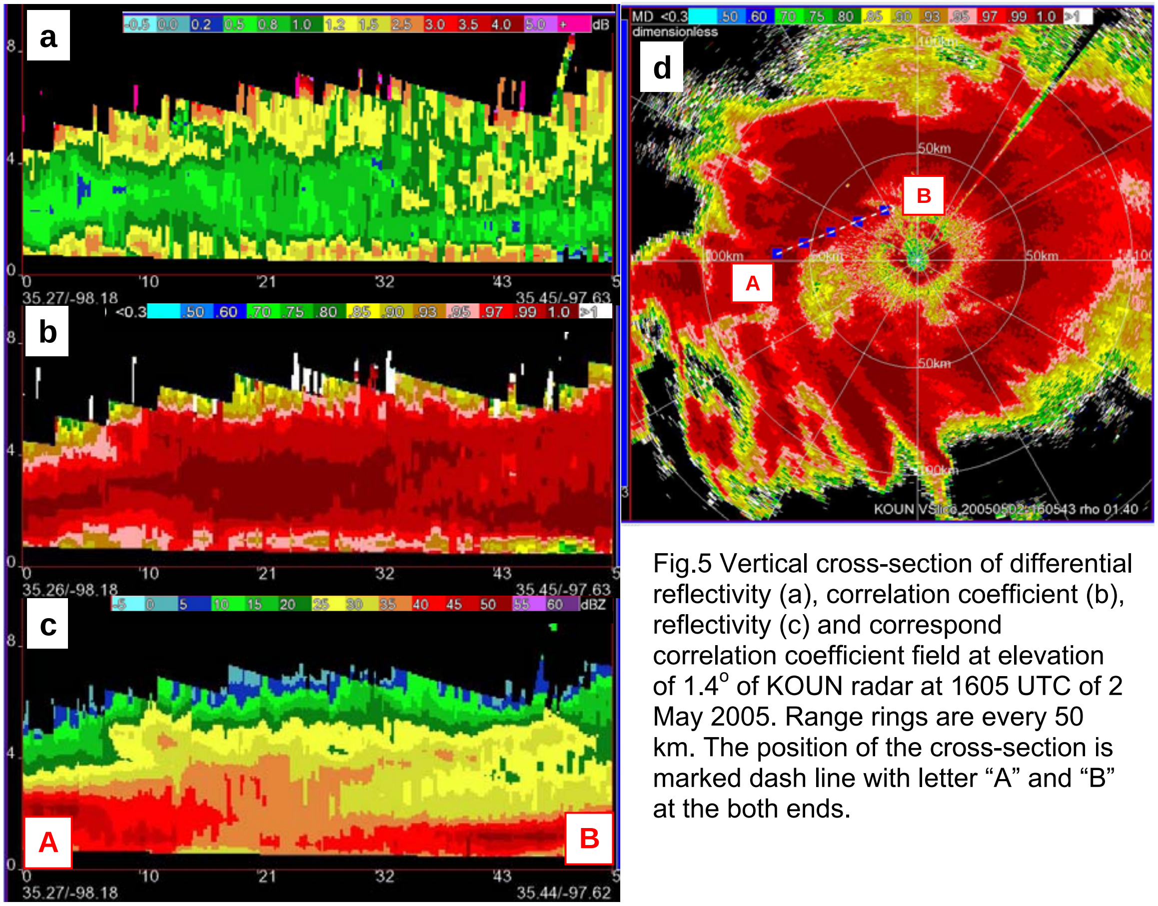

Fig.5 Vertical cross-section of differential reflectivity (a), correlation coefficient (b), reflectivity (c) and correspond correlation coefficient field at elevation of 1.4^o of KOUN radar at 1605 UTC of 2 May 2005. Range rings are every 50 km. The position of the cross-section is marked dash line with letter "A" and "B" at the both ends.

is observed. Generally, the vertical structure of polarimetric variables in Fig.5 matches well the conceptual model in Fig.4.

2.3 KH wave modulation

The vertical cross-section (see Fig. 6) is selected to be perpendicular to a KH wave and also along a radar beam, so the Doppler velocity Vr almost fully represents the velocity projected onto this cross-section. The length (from point A to B) of this cross-section is 54 km. It is long enough to cover an entire KH wave and its evolution within three volume scans (~13 min). Evolution of the fields of Vr, ρ_{hv}, Z_{dr}, and reflectivity in a vertical cross-section is illustrated in Fig.7. The Vr field clearly exhibits a recirculating region indicated by red circle with arrows inside KH billow. Green color stands for the Doppler velocity toward to the radar and red color means velocity away from the radar. KOUN radar is at the point B side in Fig.7. The white arrows in the figure show the flow direction. The flow is from right hand side (RHS) to left hand side (LHS) in the bottom layer, and from LHS to RHS in the top layer.

In order to better explain the microphysical structure of this KH wave, a diagram of one KH wave is plotted and shown in Fig.8. The wave is divided into three regions A, B, and C. Region A is the top layer of the wave and region B is the bottom layer. Region C is in the middle of the wave.

The high ρ_{hv} (~1.0), low Z_{dr} (~0.5dB), and moderate reflectivity (~30 to 35dBZ) (see Fig.7) in the recirculating region (region C) indicate the hydrometeors are dry aggregated snowflakes. From region C to region A, reflectivity gradually decreases from 35dBZ to 15dBZ separately. Meanwhile, Z_{dr} gradually increase from 0.5dB to about 2.5dB. It means that the type of hydrometeors changes from heavily aggregated snow flakes to lightly aggregated snowflakes and ice crystals. Thus, the KH wave modulates the deposition and aggregation layers (see Fig.8). It also traps and lifts a certain amount of aggregated snow inside KH waves. Because the reflectivity is

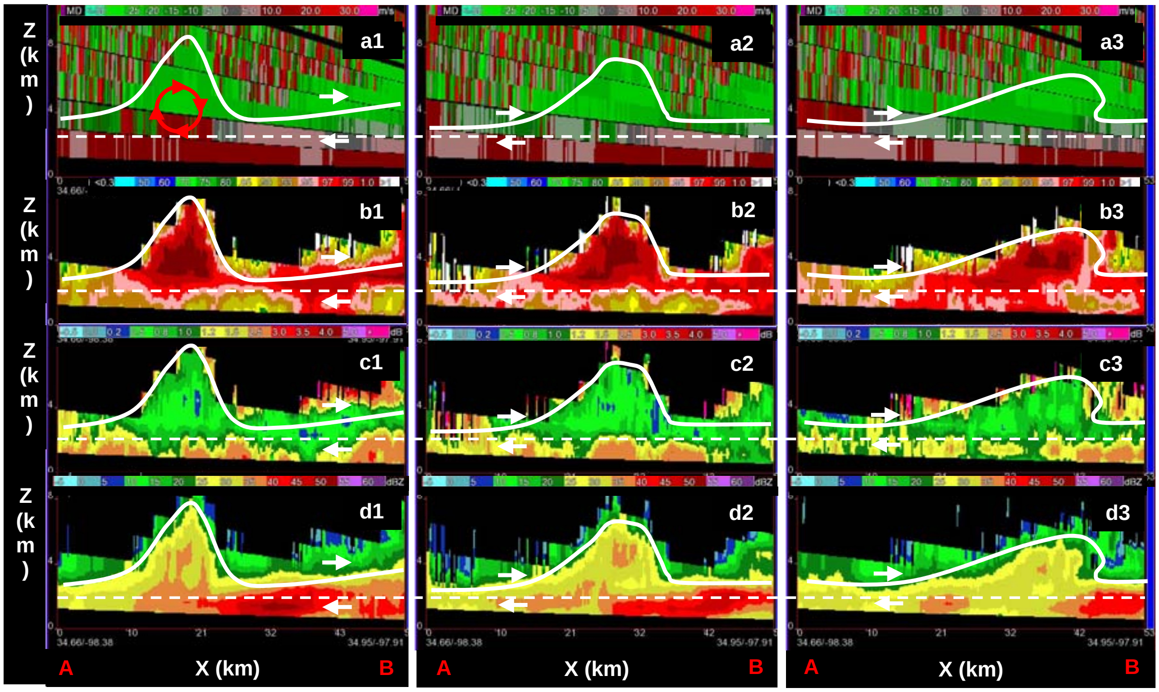

Fig.7 Evolution of the fields of polarimetric variables, (a) Vr, (b) ρ_{hv}, (c) Z_{dr}, and (d) reflectivity at the same vertical cross-section as shown in Fig.4 at 16:05 UTC (1st column), 16:12 UTC (2nd column), and 16:18 UTC (3rd column). The white solid lines outline the shape of KH waves. The white dash lines indicate the height of 0^{o}C observed by OUN rawinsonde. The white arrows show the flow directions. The red circle and arrows in a1 display the recirculation and its direction inside the wave.

proportional to the sixth moment of the scatterer size, the increase of reflectivity in region C shown in Fig.7d1 and d2 might indicate that recirculating in region C provides more opportunities for snowflakes to aggregate and grow.

The series of images in Fig.7 also clearly exhibits the evolution of the KH wave from mature stage to wave breaking. As the amplitude of wave further increases, the nonlinear effects become stronger and stronger. They cause the crest of the wave "curling over" and breaking as shown in the 2nd and 3rd columns in Fig.7. Due to the decrease of wave amplitude, region C becomes smaller. A "tail" of high ρ_{hv} and reflectivity with low Z_{dr} indicates that some of aggregated snow flakes are "squeezed out" from region C and left behind. Then the wave continues breaking

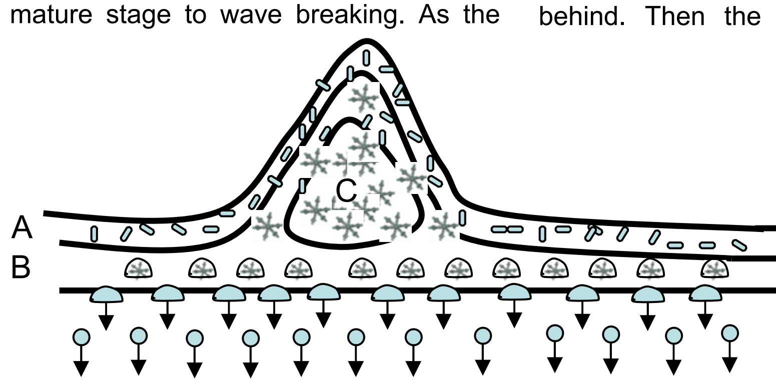

Fig.8 Modulation of stratiform precipitation by the KH wave.

down and becomes more flat. More snowflakes are released from region C. High ρ_{hv} and relative low reflectivity beneath the wave (see Fig.7b3 and d3) indicate that the melting layer is broken here due to this quite strong release. There may be two reasons for the broken of melting layer. One is that the snowflakes with the upper level cold air (below 0^{o}C) is released in a relative fast speed from region C, so this blob of cold air have not fully mixed with ambient warm air (above 0^{o}C) and its temperature is still slightly below 0^{o}C. The snowflakes inside this blob of air are not melted. The other reason is that the amount of trapped snowflakes is relative large. The melting of portion of these particles cools down the surrounding air and slows down the further melting process. Thus, the particles in this region may be the mixture of melted and unmelted snowflakes.

3. Conclusions

The evolution of a series of well defined KH waves observed by polarimetric prototype of WSR-88D radar in a stratiform precipitation is documented and analyzed in this paper. The dynamic characteristics of the waves are consistent with previous studies. There is evidence that the top layer of the cloud is modulated by KH waves due to periodic up and down movement. This study has also proved the capability of polarimetric radar to detect the fine microphysical structure inside the storm. This capability will help us with better understanding of the dynamics and microphysics of the storm development.

Reference

Browning, K.A.: 1971: Structure of the Atmosphere in the Vicinity of Large-Amplitude Kelvin-Helmholtz Billows. *Quart. J. Roy. Meteorol. Soc.* **97**, 283-299

Houze, R. 1993: Cloud Dynamics. *Academic Press*. 572pp.

Rottman, J. W. and Smith, R.B., 1989: A laboratory model of severe downslope winds. *Tellus*. **41A**, 401-415.

Ryzhkov, A. V., D. S. Zrnic, 2003: Discrimination between rain and snow with a polarimetric NEXRAD radar. Preprints, 31st International Conference on Radar Meteorology, Seattle, WA, USA, American Meteorological Society, 635-638.

Zrnic, D. S., N. Balakrishnan, C. Ziegler, V. Bringi, K. Aydin, T. Matejka, 1993: Polarimetric signatures in the stratiform region of a mesoscale convective system. Journal of Applied Meteorology, **32**, 678-693.